Desalination and Water Treatment
www.deswater.com

doi: 10.5004/dwt.2019.24054

155 (2019) 216–224
July

NiO powder synthesized through nickel metal complex degradation for water treatment

Thangavelu Kavitha[a,b,*], Shanmugam Kumar[a], Veena Prasad[b], Abdullah M. Asiri[c,d], Tahseen Kamal[c,d], Mazhar Ul-Islam[e,*]

[a]*Department of Mechanical and Materials Engineering, Khalifa University of Science and Technology, Masdar Institute, Masdar City, P.O. Box 54224, Abu Dhabi, UAE, emails: kavichemistry@gmail.com (T. Kavitha), s.kumar@eng.oxon.org (S. Kumar)*
[b]*Department of Chemistry, Centre for Nano and Soft Matter Sciences, 1329, Jalahalli, Bangalore-560013, India, email: veena@cens.res.in (V. Prasad)*
[c]*Department of Chemistry, Faculty of Science, King Abdulaziz University, Jeddah 21589, Saudi Arabia, emails: aasiri2@kau.edu.sa (A.M. Asiri), tkkhan@kau.edu.sa (T. Kamal)*
[d]*Center of Excellence for Advanced Materials Research, King Abdulaziz University, Jeddah 21589, Saudi Arabia*
[e]*Department of Chemical Engineering, College of Engineering, Dhofar University, Salalah, Oman, email: mulislam@du.edu.om (M. Ul-Islam)*

Received 18 September 2018; Accepted 1 March 2019

ABSTRACT

This study was aimed to synthesize nickel oxide (NiO) powder and its subsequent use in bactericidal activities by exploring the role of interaction at nanoparticle-bacteria interface of *E. coli* (gram negative) microorganism as well as water treatment by catalysing the two toxic azo dyes reduction reactions by sodium borohydride. The NiO nanoparticles were synthesized through single-step, residue free, in situ thermal decomposition method. Their size, structural and morphological features were confirmed through various analytical tools. An average size of 7–8 nm, high crystallinity and cubic crystal structure of the synthesized nanoparticles was confirmed by XRD and HR-TEM analyses. The NiO nanoparticles revealed virtuous bactericidal activities against pathogenic *E. coli*. Field emission scanning electron microscopy images were used as the evidence of the cell wall deterioration. The prepared NiO nanoparticles were also used in the catalytic reduction reactions of methyl orange (MO) and congo red (CR) dyes by sodium tetra-borohydrate. The reaction rate constants for the MO and CR were 0.4989 and 0.298 min^{-1}, respectively. The reaction mechanism, comparison with other catalyst and recyclability of the NiO were discussed.

Keywords: NiO nanoparticles; Antibacterial; Catalyst; Pollutants reduction; $NaBH_4$

1. Introduction

The two threats posed on the human lives are the toxic pollutants and certain un-friendly microorganisms [1–10]. Basically, men themselves are responsible for the pollutants cause [3]. Among the different type of pollutions, toxic chemicals used in the industries are sometimes discharged without proper treatment. For instance, colouring compounds and dyes from different industries are drained in the form of their aqueous solutions into the nearby streams [11,12]. These compounds impose an adverse effect on the aquatic lives directly and on human lives indirectly. Some of the examples of such toxic compounds discharged by textile, pharmaceutical, leather and printing industries are azo functional group containing dyes, nitroaromatic compounds and heavy metal ions etc. The easiest approaches

* Corresponding authors.

for their removal are the adsorption assisted extraction from the aqueous environment or their complete reduction in short time by using suitable reductants and catalysts [13–15]. The latter method has advantage of complete chemical structure change of the pollutant [15]. In-fact noble metal nanoparticles have been considered efficient catalyst but their high cost is the main hurdle in their utilization as catalyst. Transition metal nanoparticles are also efficient catalyst but they are highly unstable. Therefore, stable oxide nanoparticles of various metals such as zinc, copper silver and nickel have been synthesized and used in catalysing different reactions [16–19].

To fight against the un-friendly microorganisms, antimicrobial studies on developed materials are often performed. Antibacterial activity is the ability to kill bacteria or slowing down their growth, without affecting the neighbouring tissues or cells. The materials with antibacterial properties are prime important in medicine, water treatment, textile and food packaging industry [20–22]. In particular, antibacterial agents are considered paramount to combat against various diseases. Even then, the bacterial resistance to antibacterial drugs has increased and became a common phenomenon, which is a primary problem in a global health concern [23,24]. The possible reason lying behind the bacterial resistance could be due to evolutionary processes in antibiotic therapy namely transduction and horizontal gene transfer by conjugation [25,26]. The resistant species are known as superbugs which lead to the evolution of diseases that were controlled for a long time. The bacterial strains causing tuberculosis could be stated as the better example in this aspect as it is approximated that nearly half a million new cases of multidrug-resistant tuberculosis appear globally during each year. Also, Delhimetallo-b-lactamase-1 enzyme, is accountable for bacterial resistance to all standard intravenous antibiotics for the treatment of severe infections [27]. Hence, infectious diseases persist to be one of the superior health threats all over the world. Also, the disadvantages of conventional organic antimicrobial compounds are their adverse side effects during prolong use, toxicity due to high dose, irritability and less stability at high temperature or pressure.

As alternatives to organic compounds based antibacterial agents, the research in treatment of bacterial infections using bloomed nanomaterials as novel and efficient antimicrobial agents has recently increased. In nano-meter scale, the chemical, mechanical, electrical, structural, morphological and optical properties of the material is modified/enhanced due to greater number of atoms at their surface and thus high surface reactivity easing the interaction with any moiety and here biomolecules or cells thus, assisting the engulfing of nanoparticles into cells [14,22,28]. The antimicrobial effectiveness of nanoparticles rely upon their physiochemical properties namely composition, surface modification, particle size and finally, also on kind of bacterial species used for the study (cell). The exact mechanisms for antibacterial activity of nanoparticles are still under research, yet free metal ion toxicity and oxidative stress via the generation of reactive oxygen species (ROS) are the most popular proposed possibilities in this regard [29,30]. The metal and metal oxide nanoparticles tested for antimicrobial activity are Au, Ag, Si, Ag_2O, TiO_2, CuO, ZnO, CaO, CeO_2 and MgO [31,32]. Besides, due to extensive use of nanoparticles, uncontrolled release of these nanoparticles into the environment would become inevitable [3,33].

Nickel oxide (NiO) is an inorganic p-type semiconductor of great attention with a large bandgap and deep valence band that lines up with the highest occupied molecular orbital levels of many p-type organic semiconductors and electrochromism. Therefore, its use as a hole transporting layer in organic optoelectronic devices and organic light-emitting diodes [34,35]. Moreover, it has been widely used in solar cell, capacitor, and rechargeable lithium ion batteries [36], and in smart windows, sensors and electrochemical super capacitors [37]. Different methodologies such as the precursor thermal decomposition method, calcination, the template method, the chemical precipitation method and the aqueous solution methods have been reported to produce NiO nanoparticles [37–40]. In few studies, NiO nanoparticles have been prepared by the direct high temperature treatment of Ni-based complexes synthesized by the reaction of Ni^{2+} ions with *o*-mercaptobenzoic acid [41], supercritical water treatment [42], glycine-nitrate combustion using nanocrystalline cellulose as template [43], hydrogel and cellulose filter paper as supports [44,45] and a green approach of using plant extract of plant *Monsonia burkeana* [46]. Moreover, till date; most of the available methods of nanoparticles synthesis methods have some limitations due to complex procedures, uneconomical and low yield, tedious procedures, special conditions or complex apparatus, and high cost.

In this research study, we explored the NiO nano-powders antibacterial activity with its mechanism and biocompatibility tests. Towards this purpose, thermal decomposition of nickel(II) benzoate dihydrazinate an organometallic complex was used to prepare NiO nano-powders. The surface charge of NiO nanoparticles studied by zeta potential bestowed the electrostatic mode of attachment of the same on the cell wall. The prepared NiO nanoparticles through thermal decomposition of a nickel complex was also used as catalyst in the reduction reactions. The catalytic properties of the NiO in these reduction reactions were discussed and comparatively presented with some recent reports.

2. Experimental setup

2.1. Materials

Hydrazine hydrate, nickel (II) nitrate hexahydrate, benzoic acid and ethanol, were purchased from Sigma–Aldrich. Congo red and methyl orange and $NaBH_4$ were bought from Loba Chemie, India. These chemicals were used and received without further processing. Growth media for *E. coli* were obtained from Debco.

2.2. Synthesis of NiO nanoparticles

The aqueous solution of nickel (II) nitrate hexahydrate (0.01 mol) was mixed in-situ with hydrazinium benzoate (0.02 mol) and the subsequent mixture was concentrated to 30% of its aggregate volume. After this, the reaction mixture was cooled, and the solids formed were separated by

filtration. The obtained solids were washed with ethanol to remove the unreactive components and dried. The complex formed of nickel benzoate dihydrazinate consequently decayed into NiO nanoparticles when heated at 200°C for an hour.

2.3. Characterization

0.1 % (w/v) NiO nanoparticles were suspended in an ethanol solvent by sonicating for 1 h. Then a small drop of this solution was deposited on a TEM grid. Size and structure of synthesized nanoparticles was confirmed through transmission electron microscopy (TEM), performed on a JEOL JEM-2100 microscope. The instrument was operated at ultra-high resolution voltage of 200 kV. X-ray diffraction patterns were obtained from the prepared sample using an X-Ray diffractometer (X0Pert-APD PHILIPS, Netherland) with an X-ray generator (3 KW) and anode (LFF Cu). The Cu *Kα* radiations with wavelength of 1.542 A° were used while X-ray generator current and voltage were 30 mA and 40 kV, respectively. The scanning angle in the X-ray diffractometer was varied from 10 to 70°. Zeta potential were measured through a Malvern Zetasizer Nano instrument (Nano-ZS90, England). The instrument uses a laser wavelength of 633 nm under the Smoluchowski approximation. Final data was an average of three individual measurements. A uv-visible spectrophotometer was used in the catalytic reductions reactions by measuring the absorbance of the dye solutions.

2.4. Antimicrobial activity

Antibacterial activities of NiO nanoparticles were made against *E. coli* through colony-forming unit (CFU) count method following the procedure reported earlier [1]. Briefly, 0.003 g NiO nanoparticles were added to various test tubes. The tubes were then seeded with 1 mL fresh cultures of *E. coil* and incubated at 37°C at 150 rpm for 1, 2 and 3h. Afterwards 100 μL of each sample from tubes were spread on plates containing *E. coli* agar media. These plates were incubated at 37°C for 18 h. After incubation, colonies were counted and results between plates were compared.

2.5. Catalytic activity tests

Catalytic activity of the synthesized nanoparticles was determined by reduction reactions of two dyes containing azo functional group. The two dyes were congo red (CR) and methyl orange (MO). We used the reported method for the catalytic reduction of theses dyes [11,47,48]. Stock solutions of the two dyes were prepared with concentrations of 0.12 mM. The dye was then filled to a uv cell of 3.5 mL. The volume of dye was always 2 mL. The reductant aqueous solution amount was 1 mL which was introduced to the dye solution containing uv cell. Its concentration was 0.1 M. The sodium borohydride solution was always freshly prepared and subsequently used. An initial uv-vis spectrum was recorded from the dye + reductactant solution. The solution was remained for some time to check the reducibility of the dyes by $NaBH_4$. It was found that the reaction was quite slow as no change in color was observed. As soon as the NiO nanoparticles (8 mg) were added to the UV cell, the reaction started which was monitored using continuous recording of the UV-vis data.

3. Results and discussion

Fig. 1 portrays the synthesis of NiO nanoparticles in a non-hydrolytic way i.e. by thermal decomposition of nickel benzoate dihydrazinate complex. The central reason for choosing this complex revolves around two reasons: the exothermic disintegration of hydrazine helps in the development of nanoparticles at generally low temperature and the scattering of metal particle in 3D coordination circle permits the arrangement of fine particles after deterioration. In addition, thermal decomposition method gives the end product with no purity in a simple way. This approach is based on a previously reported method for preparing NiO nanoparticles [49], but it was notably modified with respect to temperature to see any changes in morphology. Herein, we obtained NiO nanoparticles which could be an effective bactericide due to large surface area compared to nanorods.

The structural and morphological characteristics of NiO nanoparticles were identified using XRD and TEM as shown in Fig. 2. First, the XRD pattern (Fig. 2(a)) shows a little broad diffraction peaks indicating the well crystalline nature of the NiO nanoparticles. The broadness of the peaks might be due to the nano-sized particles of the NiO powders. The three peaks appearing at 2θ = 37.096°, 43.099°, 62.593°, correspond to the (111), (200), (220) planes of cubic crystal structure of NiO, respectively [37]. No peaks due to any other Ni analogue or impurities were found from XRD, indicating the complete decomposition of nickel benzoate dihydrazinate complex to NiO at elevated temperature of 200°C for 1 h. The images of the morphology and microstructures observed by TEM shown in Figs. 2(b) and (c) clearly manifest that as-synthesized NiO nanoparticles has an average size of around 7–8 nm. The HR-TEM image in Fig. 2(d) confirms that the synthesized NiO nanoparticles have a cubic crystal structure, of which the interplanar spacing of 0.221 nm agreeing to (111) lattice planes of the cubic rock salt NiO in just one simple step of thermal decomposition. The ring structure in SAED of NiO nanoparticles conveyed the highly crystalline NiO nature and the patterns can be readily indexed to (111), (200) and (220) reflection planes of FCC NiO nanoparticles.

To validate the mode of interaction at NiO nanoparticle-bacterial interface we measured zeta potential of NiO nanoparticles as a function of pH as shown in Fig. 3. At acidic pH, the surface of NiO nanoparticles bears a positive charge whereas at basic pH it exhibits a negative charge.

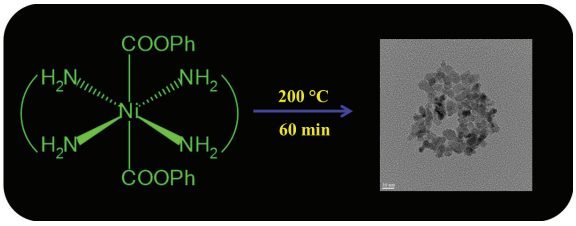

Fig. 1. Schematic representation of the NiO nanoparticles synthesis.

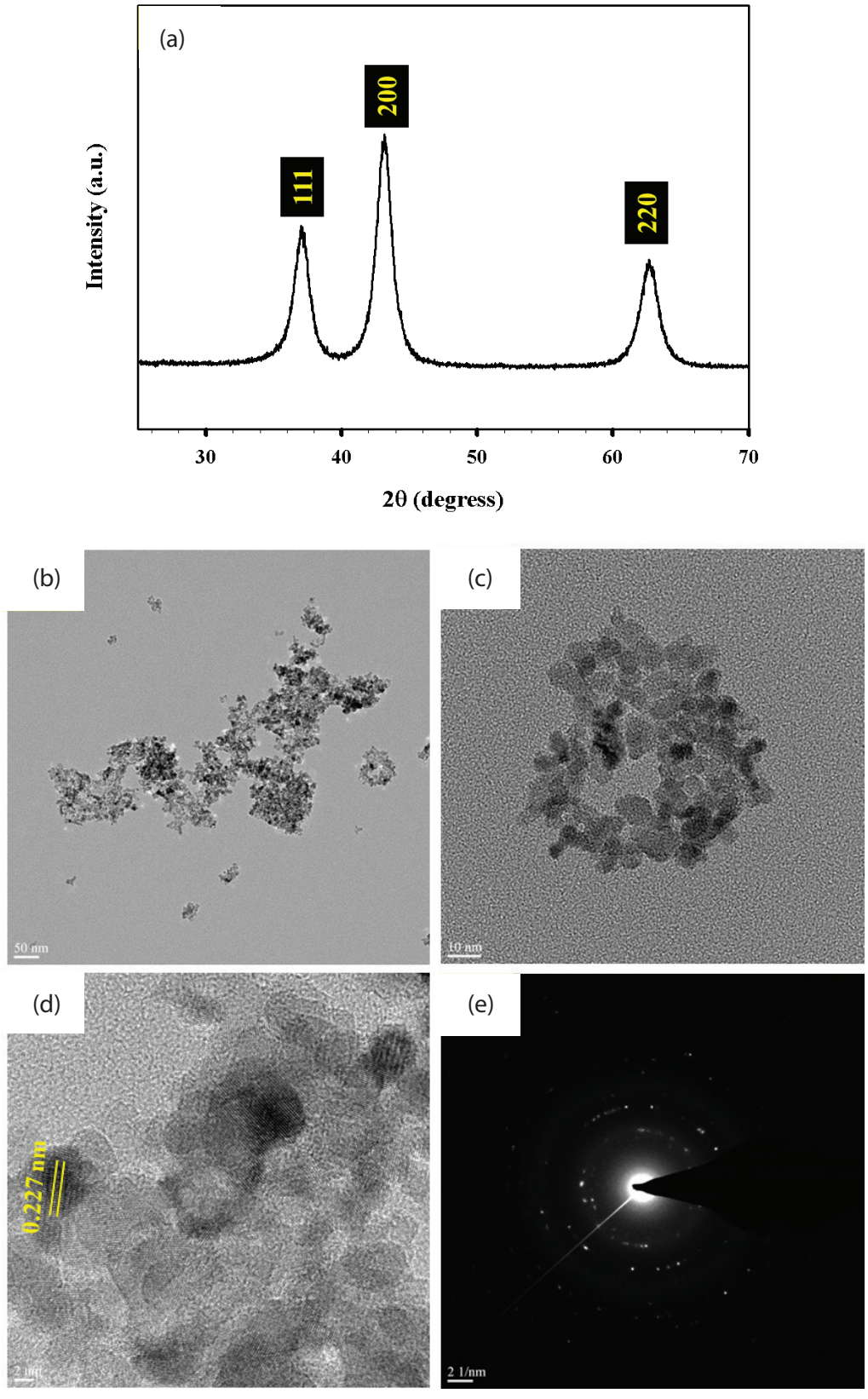

Fig. 2. NiO nanoparticle's (a) XRD pattern, (b) and (c) TEM, (d) HR-TEM images and (e) the SAED pattern.

The chemistry behind such change with pH is protonation/deprotonation of surface group. In acidic environment, NiO nanoparticles carries a positive surface charge due to protonation and in basic environment deprotonation gives negative surface charge [50]. The pH of our interest 6–7 happens to be isoelectric point of NiO nanoparticles. The attachment of bacteria on any surface can happen via number of non-specific interactions like electrostatic, dipole-dipole, H-bond, hydrophobic and van der Waals [51]. At pH of 7, NiO nanoparticles carries a charge of −7.30 mV, so electrostatic repulsion arise between NiO nanoparticles and bacterial surface (*E. coli* surface charge= −7.20 mV at pH 6.5 [52], and hence we foresee, hydrophobic and van der Waals kind of interactions at NiO nanoparticle-bacterial interface.

NiO nanoparticles antimicrobial activity was tested against *E. coli* as they are most common pathogen. The respective bacteria were cultured with 3 μg/ml of NiO nanoparticles for 18 h and then viable bacteria were monitored by culturing in agar plates for 1, 2 and 3 h and counting the number of colony-forming units (Fig. 4). The untreated control culture has high tally of microorganisms and with time of incubation its development was colossal. It can be seen that with NiO the viability lessened nearly by 78% for *E. coli* after 1 h of treatment and with additional time of gestation there is very little development of microscopic organisms. The bactericidal features of nanomaterials and their mechanism are well-known and small particle size enhances the bactericidal efficacy [53]. It can be seen clearly that there is no noticeable bacterial cell growth for 60 and 120 min while after 180 min of incubation, there is significantly less development.

The structure and properties of bacterial cell wall plays a crucial role in diffusion of nanoparticles and hence the tolerance and susceptibility of bacteria. For clear understanding of antibacterial activity of NiO nanoparticles we intrigued the morphological changes of the bacteria as manifested in Fig. 5. The untreated control sample of *E. coli* has rod shape and the cell membrane was intact with smooth and normal surface morphology. After the treatment with NiO nanoparticles for 30 min, the cell membrane was wrinkled and ruptured with severe change in morphology of cell. These changes in surface morphology suggest the antibacterial activity of NiO nanoparticles could be through the membrane-dependent bacterial disinfection. The observed bactericidal features are in accordance with some previous reports [52,54].

CR (chemical structure in Fig. 6(a)) is considered as a stable toxic organic dye. Due to the presence of an azo functional group (–N=N–), it is also named as an azo toxic dye. It has been reported that it is widely used in different

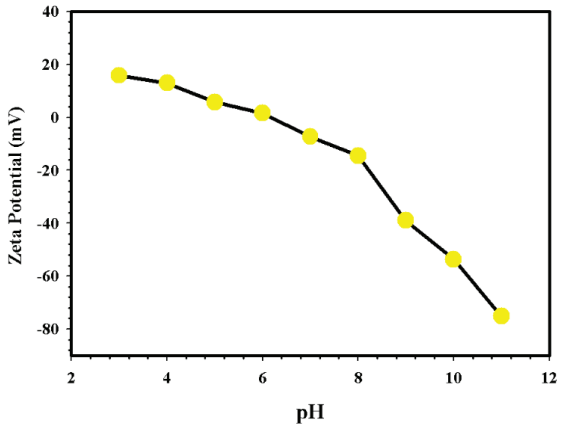

Fig. 3. Zeta potential of NiO nanoparticles as a function of pH.

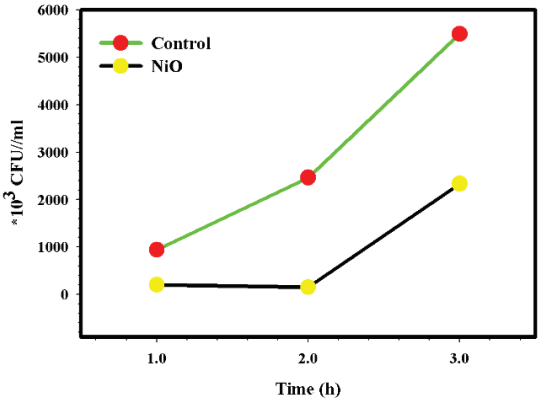

Fig. 4. NiO nanoparticles antimicrobial activity against *E. coli* for 1, 2 and 3 h.

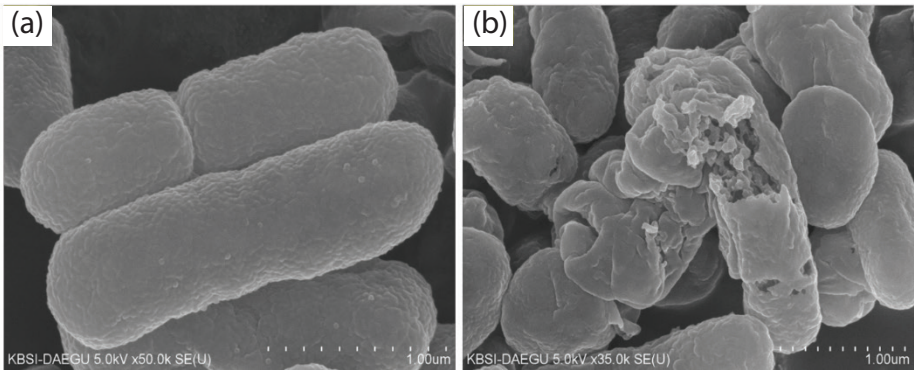

Fig. 5. FESEM images of (a) and (b) *E. coli*, control and after being treated with NiO nanoparticles for 30 min, respectively.

industries (textiles, plastics and paper) as a coloring agent [47]. Fig. 6(b) shows the uv-vis spectra of CR during its treatment with the $NaBH_4$ in the presence of NiO nanoparticles. It is clear from the initial spectrum of the CR that two peaks appeared at the 342 and 490 nm in the uv-vis region. These peaks were due to the forbidden (n–π^*) and allowed (π–π*) transitions of the azo groups present in the CR molecular structure. The addition of the reducing agent solution to the CR containing solution caused a slight decrease in the intensity of both the peaks in the UV-vis spectrum. This decrease in intensity was due to the dilution effect. Slight after the addition of the NiO nanoparticles to the reaction medium, the UV-vis spectral data were continuously recorded. A continuous decrease in the intensity of peak located at 490 nm was observed. At the same time, a new peak centered at 288 nm was also appeared. The new peak appearance was due to the sigma–d* transition which indicates the reduced form (–NH–NH–) of the azo group in the dye molecules. The time taken by the catalyst to reduce the CR dye was 9 min as noted from the nearly complete vanishing of the peak intensity at 490 nm. For the kinetic analysis of this reaction, the peak values at 490 nm were noted as A_t (absorbance at time t) except the initial reading after addition of the $NaBH_4$ as A_0. The data was treated according to the following equation of pseudo-first order kinetics,

$$\ln(C_t/C_0) = \ln(A_t/A_0) = -k_{app}t \quad (1)$$

where C_t, C_0 and k_{app} represent the concentration of the CR dye at time t, at time zero (before the beginning of the reduction reaction) and rate constant of the reaction. The k_{app} was calculated from the slope of the plot between $\ln(A_t/A_0)$ and t. This plot has been shown in Fig. 6(c). The determined rate constant of the reaction was 0.298 min^{-1} with the r^2 being 0.817.

MO (chemical structure shown in Fig. 7(a)) is another azo dye which is vastly used in common chemical laboratories and different industries. This dye causes an environmental pollution when comes to the outer world. Fig. 7(b) represents the MO reduction profiles using $NaBH_4$ in the presence of

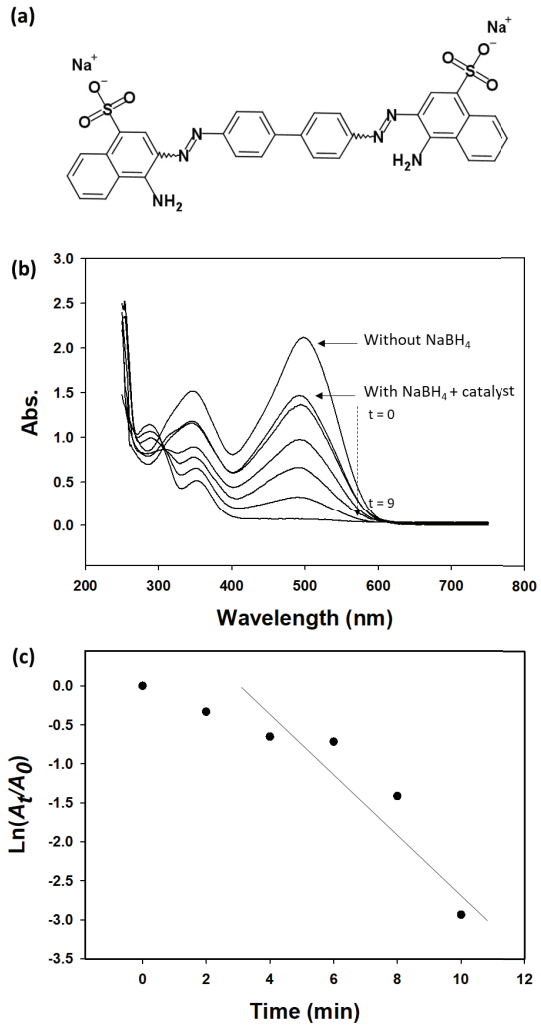

Fig. 6. The reduction reaction of CR by $NaBH_4$: (a) Chemical structure of CR, (b) uv-vis spectra of the reaction and (c) the absorbance ratio vs. time plot the reaction.

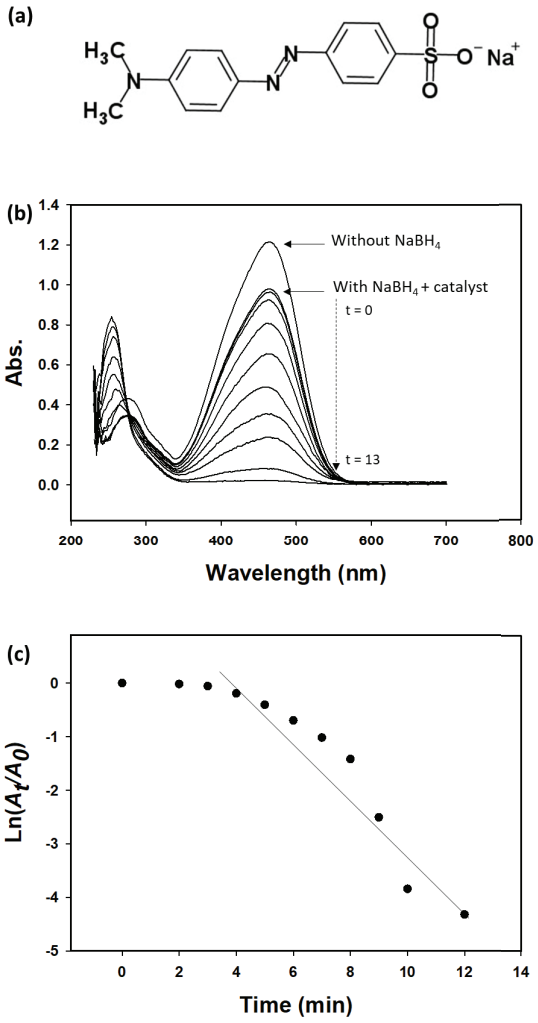

Fig. 7. The reduction reaction of MO by $NaBH_4$: (a) chemical structure of MO, (b) uv-vis spectra of the reaction and (c) the absorbance ratio vs. time plot the reaction.

NiO nanoparticles as catalyst. The uv-vis spectrum at the beginning of reduction reaction has λ_{max} at 464 nm. The intensity of this characteristics peak gradually decreased with time. Moreover, a new peak also appeared at 247 nm. This appearance was due to the hydrazine derivative. The degradation efficiency was more than 75% after 6 min of the reduction reaction. To determine the kinetic rate constant of the MO reduction reaction, the uv-vis data was treated using equation 1 similar to that of the CRs' data and shown in Fig. 7(c). The determined rate constant of the reaction was 0.498 min^{-1}. We also compared our results with the literature available reports in Table 1. Kamal et al. reported that the CR reduction reaction proceeded with a rate constant of 0.2683 min^{-1} using copper nanoparticles-chitosan coated filter paper catalyst [47]. Similarly, a rate constants of 0.3308, 1.7 × 10^{-3} s^{-1}, 0.559 and 2.1 × 10^{-3} were reported for Co-Cu/ZnPC-Chitosan nanocomposite [21], gold nanoparticles synthesized using 5,7-dihydroxy-6-metoxy-3',4' methylenedioxyisoflavone (Dalspinin) obtained from *Dalbergiacoromandeliana* roots [55], Ag and Pt Nanoparticles [56], and nanoporous gold [57]. The extra high values of the rate constants in some of those reports were due to the extremely small particle size of their catalyst.

Fig. 8 shows the reaction mechanism for the dye reduction reaction by $NaBH_4$ using NiO nanoparticles catalyst. The dye molecules and borohydride ions (BH_4^{+1}) approaches to the catalyst surface. They are adsorbed on the catalyst surface. The BH_4^{+1} acts as a carrier of hydrogen. The hydrogen attacks the dye molecules after the BH_4^{+1} transfer electrons from them to the catalyst [58]. As a result of electron carriers, the catalyst nanoparticles activate the –N=N– bonds in the dye molecules. The dye solution becomes colorless due to first the –N=N– to –HN–NH–. The hydrogenated product is diffused out of the catalyst surface and mix into the bulk solution while leaving behind the surface available for another dye molecule. It has been reported that compare to the CuO, Fe_2O_3, and Co_3O_4, the NiO is not an efficient catalyst for some other molecules hydrogenation due to its high band gap [59]. However, in the mixed or supported form, NiO outperform in the catalytic reduction reactions [60]. In the current study, the high catalytic activity of the NiO nanoparticles in the azo dye reduction reactions might be due to the presence of the carbon residue from the thermal decomposition reaction of the Ni metal complex.

The reusability tests are quite important in catalysis. These tests determine the service life and help reduce the overall cost of the reaction by introducing it in same kind of reaction for several times. Fig. 9 represents the k_{app} of the CR and MO reduction reactions by using same amount of the NiO nanoparticles as catalyst. Each reaction was proceeded with the same amount of catalyst recovered by centrifuging the reaction solution. It can be seen that the reaction rate constant was almost similar to the initial value which suggest no loss of the catalytic activity upon using it in cyclic manner.

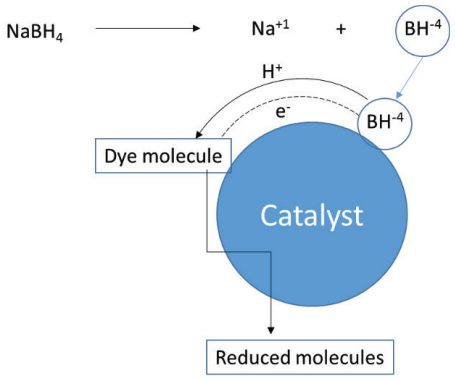

Fig. 8. Mechanism for the dye reduction reactions by $NaBH_4$.

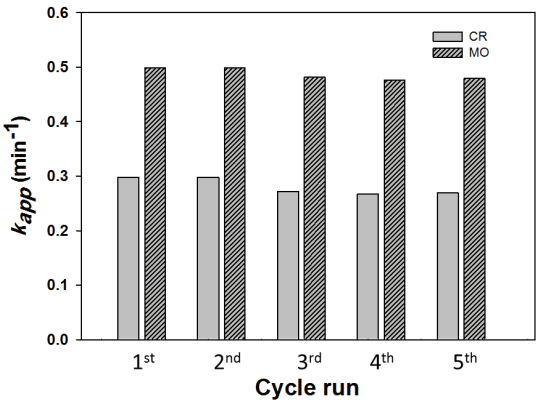

Fig. 9. Recyclability tests; reaction rate constants during multiple runs of the same NiO nanoparticles catalyst in reduction reactions.

Table 1
Comparison of the NiO catalyst with literature reports

Catalyst	Rate constant (min^{-1})	References
Co-Cu/ZnPC-Chitosan nanocomposite	0.3308	Ali et al. [21]
Gold nanoparticles	1.7 × 10^{-3a}	Umamaheswari et al. [55]
Copper nanoparticles-chitosan coated filter paper	0.2683	Kamal et al. [47]
Pt nanoparticles	0.0029	Gupta et al. [56]
Ag nanoparticles	0.5853	Gupta et al. [56]
Nanoporous gold	2.1 × 10^{-3}	Hakamada et al. [57]
NiO nanoparticles	0.4989	This study

[a]The value was reported in s^{-1} units.

4. Conclusions

In a summery, we have synthesized NiO nanoparticles by thermal decomposition technique at a comparatively moderate temperature and concentrated on the utilization of NiO nanoparticles as a viable and potential antibacterial agent against *E. coli*. The broad peaks in the XRD pattern of the combusted product suggested the nano-sized NiO particles which were further verified using TEM analysis. The data, altogether, indicated that the interaction pattern at the nanoparticle-bacteria interface is the curtain-raiser in determining the antimicrobial activity of NiO nanoparticles. The NiO nanoparticles also outperformed in catalysing the two pollutants reduction reactions. These outcomes suggested the potential use of NiO nanoparticles in beauty care products, water treatment, biomedical and other modern areas.

References

[1] T. Kavitha, S. Haider, T. Kamal, M. Ul-Islam, Thermal decomposition of metal complex precursor as route to the synthesis of Co3O4 nanoparticles: Antibacterial activity and mechanism, J. Alloys Compd., 704 (2017) 296–302.

[2] T. Kamal, I. Ahmad, S.B. Khan, A.M. Asiri, Synthesis and catalytic properties of silver nanoparticles supported on porous cellulose acetate sheets and wet-spun fibers, Carbohydr. Polym., 157 (2017) 294–302.

[3] T. Kamal, S.B. Khan, A.M. Asiri, Nickel nanoparticles-chitosan composite coated cellulose filter paper: An efficient and easily recoverable dip-catalyst for pollutants degradation, Environ. Pollut., 218 (2016) 625–633.

[4] F. Ali, S.B. Khan, T. Kamal, K.A. Alamry, A.M. Asiri, Chitosan-titanium oxide fibers supported zero-valent nanoparticles: highly efficient and easily retrievable catalyst for the removal of organic pollutants, Sci. Rep., 8 (2018) 6260.

[5] F. Ali, S.B. Khan, T. Kamal, K.A. Alamry, A.M. Asiri, T.R.A. Sobahi, Chitosan coated cotton cloth supported zero-valent nanoparticles: Simple but economically viable, efficient and easily retrievable catalysts, Sci. Rep., 7 (2017) 16957.

[6] F. Ali, S.B. Khan, T. Kamal, Y. Anwar, K.A. Alamry, A.M. Asiri, Bactericidal and catalytic performance of green nanocomposite based-on chitosan/carbon black fiber supported monometallic and bimetallic nanoparticles, Chemosphere, 188 (2017) 588–598.

[7] T. Kamal, N. Ali, A.A. Naseem, S.B. Khan, A.M. Asiri, Polymer nanocomposite membranes for antifouling nanofiltration, Recent Pat. Nanotechnol., 10 (2016) 189–201.

[8] S.A. Khan, S.B. Khan, T. Kamal, A.M. Asiri, K. Akhtar, Recent development of chitosan nanocomposites for environmental applications, Recent Pat. Nanotechnol., 10 (2016) 181–188.

[9] M. Ul-Islam, M.W. Ullah, S. Khan, T. Kamal, S. Ul-Islam, N. Shah, J.K. Park, Recent advancement in Cellulose based nanocomposite for addressing environmental challenges, Recent Pat. Nanotechnol., 10 (2016) 169–180.

[10] M.S. Ahmed, T. Kamal, S.A. Khan, Y. Anwar, M.T. Saeed, A.M. Asiri, S.B. Khan, Assessment of anti-bacterial Ni-Al/chitosan composite spheres for adsorption assisted photo-degradation of organic pollutants, Curr. Nanosci., 12 (2016) 569–575.

[11] T. Kamal, S.B. Khan, S. Haider, Y.G. Alghamdi, A.M. Asiri, Thin layer chitosan-coated cellulose filter paper as substrate for immobilization of catalytic cobalt nanoparticles, Int. J. Biol. Macromol., 104 (2017) 56–62.

[12] I. Ahmad, S.B. Khan, T. Kamal, A.M. Asiri, Visible light activated degradation of organic pollutants using zinc-iron selenide, J. Mol. Liq., 229 (2017) 429–435.

[13] T. Kamal, Y. Anwar, S.B. Khan, M.T.S. Chani, A.M. Asiri, Dye adsorption and bactericidal properties of TiO2/chitosan coating layer, Carbohydr. Polym., 148 (2016) 153–160.

[14] T. Kamal, M. Ul-Islam, S.B. Khan, A.M. Asiri, Adsorption and photocatalyst assisted dye removal and bactericidal performance of ZnO/chitosan coating layer, Int. J. Biol. Macromol., 81 (2015) 584–590.

[15] S. Haider, T. Kamal, S.B. Khan, M. Omer, A. Haider, F.U. Khan, A.M. Asiri, Natural polymers supported copper nanoparticles for pollutants degradation, Appl. Surf. Sci., 387 (2016) 1154–1161.

[16] C.-W. Tang, T.-C. Liu, R.-C. Wu, Y.-Y. Shu, C.-B. Wang, Efficient microwave enhanced degradation of 4-nitrophenol in water over coupled nickel oxide and solid acid catalysts, Sustain. Chem. Pharm., 8 (2018) 10–15.

[17] M. Seo, S.Y. Kim, Y.D. Kim, E.D. Park, S. Uhm, Highly stable barium zirconate supported nickel oxide catalyst for dry reforming of methane: from powders toward shaped catalysts, Int. J. Hydrog. Energy, 43 (2018) 11355–11362.

[18] P. Suresh, J.J. Vijaya, T. Balasubramaniam, L.J. Kennedy, Synergy effect in the photocatalytic degradation of textile dyeing waste water by using microwave combustion synthesized nickel oxide supported activated carbon, Desal. Wat. Treat., 57 (2016) 3766–3781.

[19] F. Rostamkhani, H. Karami, A. Ghasemi, Application of nickel oxide nanoparticles as reusable sorbent for the removal of lead ions from contaminated water, Desal. Wat. Treat., 60 (2017) 319–328.

[20] A. Haider, S. Haider, I.-K. Kang, A. Kumar, M.R. Kummara, T. Kamal, S.S. Han, A novel use of cellulose based filter paper containing silver nanoparticles for its potential application as wound dressing agent, Int. J. Biol. Macromol., 108 (2018) 455–461.

[21] F. Ali, S.B. Khan, T. Kamal, Y. Anwar, K.A. Alamry, A.M. Asiri, Anti-bacterial chitosan/zinc phthalocyanine fibers supported metallic and bimetallic nanoparticles for the removal of organic pollutants, Carbohydr. Polym., 173 (2017) 676–689.

[22] S.B. Khan, F. Ali, T. Kamal, Y. Anwar, A.M. Asiri, J. Seo, CuO embedded chitosan spheres as antibacterial adsorbent for dyes, Int. J. Biol. Macromol., 88 (2016) 113–119.

[23] S.B. Khan, S.A. Khan, H.M. Marwani, E.M. Bakhsh, Y. Anwar, T. Kamal, A.M. Asiri, K. Akhtar, Anti-bacterial PES-cellulose composite spheres: dual character toward extraction and catalytic reduction of nitrophenol, RSC Adv., 6 (2016) 110077–110090.

[24] N. Ali, Awais, T. Kamal, M. Ul-Islam, A. Khan, S.J. Shah, A. Zada, Chitosan-coated cotton cloth supported copper nanoparticles for toxic dye reduction, Int. J. Biol. Macromol., 111 (2018) 832–838.

[25] W. Witte, International dissemination of antibiotic resistant strains of bacterial pathogens, Infect. Genet. Evol., 4 (2004) 187–191.

[26] H.S. Nagendra Prasad, C.S. Karthik, H.M. Manukumar, L. Mallesha, P. Mallu, New approach to address antibiotic resistance: miss loading of functional membrane microdomains (FMM) of methicillin-resistant *Staphylococcus aureus* (MRSA), Microb. Pathog., 127 (2019) 106–115.

[27] M.J. Hajipour, K.M. Fromm, A. Akbar Ashkarran, D. Jimenez de Aberasturi, I.R. de Larramendi, T. Rojo, V. Serpooshan, W.J. Parak, M. Mahmoudi, Antibacterial properties of nanoparticles, Trends Biotechnol., 30 (2012) 499–511.

[28] S.A. Khan, S.B. Khan, T. Kamal, M. Yasir, A.M. Asiri, Antibacterial nanocomposites based on chitosan/Co-MCM as a selective and efficient adsorbent for organic dyes, Int. J. Biol. Macromol., 91 (2016) 744–751.

[29] A. Besinis, T.D. Peralta, R.D. Handy, The antibacterial effects of silver, titanium dioxide and silica dioxide nanoparticles compared to the dental disinfectant chlorhexidine on *Streptococcus mutans* using a suite of bioassays, Nanotoxicology, 8 (2014) 1–16.

[30] S. Liu, H. Yuan, H. Bai, P. Zhang, F. Lv, L. Liu, Z. Dai, J. Bao, S. Wang, Electrochemiluminescence for electric-driven antibacterial therapeutics, J. Am. Chem. Soc., 140 (2018) 2284–2291.

[31] S.M. Dizaj, F. Lotfipour, M. Barzegar-Jalali, M.H. Zarrintan, K. Adibkia, Antimicrobial activity of the metals and metal oxide nanoparticles, Mater. Sci. Eng. C., 44 (2014) 278–284.

[32] P.K. Stoimenov, R.L. Klinger, G.L. Marchin, K.J. Klabunde, Metal oxide nanoparticles as bactericidal agents, Langmuir, 18 (2002) 6679–6686.
[33] T.J. Baker, C.R. Tyler, T.S. Galloway, Impacts of metal and metal oxide nanoparticles on marine organisms, Environ. Pollut., 186 (2014) 257–271.
[34] Y. Zhao, H. Wang, S. Zhuang, G. Wu, J. Leng, W. Li, F. Gao, B. Zhang, G. Du, Near infrared electroluminescence from n-InN/p-NiO/GaN light-emitting diode fabricated by PAMBE, Opt. Commun., 371 (2016) 128–131.
[35] W.-T. Wu, C.-M. Hsu, W.-M. Lin, D.-H. Tsai, U.-J. Peng, Optical and electrical effects of nickel oxide interlayer for anode-recessed organic light-emitting diodes, Org. Electron., 30 (2016) 219–224.
[36] Y. Ding, D. Mu, B. Wu, R. Wang, Z. Zhao, F. Wu, Recent progresses on nickel-rich layered oxide positive electrode materials used in lithium-ion batteries for electric vehicles, Appl. Energy, 195 (2017) 586–599.
[37] T. Kamal, High performance NiO decorated graphene as a potential H2 gas sensor, J. Alloys Compd., 729 (2017) 1058–1063.
[38] J.-W. Lang, L.-B. Kong, W.-J. Wu, Y.-C. Luo, L. Kang, Facile approach to prepare loose-packed NiO nano-flakes materials for supercapacitors, Chem. Commun., 0(2008) 4213–4215.
[39] N.N.M. Zorkipli, N.H.M. Kaus, A.A. Mohamad, Synthesis of NiO nanoparticles through sol-gel method, Procedia Chem., 19 (2016) 626–631.
[40] D.-B. Kuang, B.-X. Lei, Y.-P. Pan, X.-Y. Yu, C.-Y. Su, Fabrication of novel hierarchical β-Ni(OH)2 and NiO microspheres via an easy hydrothermal process, J. Phys. Chem. C., 113 (2009) 5508–5513.
[41] F.-N. Shi, J. Jiang, H. Xiao, X. Li, An extra-long-life supercapacitor based on NiO/C&S composite by decomposition of Ni-based coordination complex, Mater. Des., 153 (2018) 203–210.
[42] M. Golmohammadi, J. Towfighi, M. Hosseinpour, S.J. Ahmadi, An investigation into the formation and conversion of metal complexes to metal oxide nanoparticles in supercritical water, J. Supercrit. Fluids, 107 (2016) 699–706.
[43] Y.-T. Foo, J.E.-M. Chan, G.-C. Ngoh, A.Z. Abdullah, B.A. Horri, B. Salamatinia, Synthesis and characterization of NiO and Ni nanoparticles using nanocrystalline cellulose (NCC) as a template, Ceram. Int. 43 (2017) 16331–16339.
[44] T. Kamal, I. Ahmad, S.B. Khan, A.M. Asiri, Agar hydrogel supported metal nanoparticles catalyst for pollutants degradation in water, Desal. Wat. Treat. 136 (2018) 190–298.
[45] I. Ahmad, T. Kamal, S.B. Khan, A.M. Asiri, An efficient and easily retrievable dip catalyst based on silver nanoparticles/chitosan-coated cellulose filter paper, Cellulose, 23 (2016) 3577–3588.
[46] P. Kganyago, L.M. Mahlaule-Glory, M.M. Mathipa, B. Ntsendwana, N. Mketo, Z. Mbita, N.C. Hintsho-Mbita, Synthesis of NiO nanoparticles via a green route using *Monsonia burkeana*: the physical and biological properties, J. Photochem. Photobiol. B., 182 (2018) 18–26.
[47] T. Kamal, S.B. Khan, A.M. Asiri, Synthesis of zero-valent Cu nanoparticles in the chitosan coating layer on cellulose microfibers: evaluation of azo dyes catalytic reduction, Cellulose, 23 (2016) 1911–1923.
[48] F.U. Khan, Asimullah, S.B. Khan, T. Kamal, A.M. Asiri, I.U. Khan, K. Akhtar, Novel combination of zero-valent Cu and Ag nanoparticles @ cellulose acetate nanocomposite for the reduction of 4-nitro phenol, Int. J. Biol. Macromol., 102 (2017) 868–877.
[49] T. Kavitha, H. Yuvaraj, A facile approach to the synthesis of high-quality NiO nanorods: electrochemical and antibacterial properties, J. Mater. Chem., 21 (2011) 15686–15691.
[50] N. Wang, C. Hsu, L. Zhu, S. Tseng, J.-P. Hsu, Influence of metal oxide nanoparticles concentration on their zeta potential, J. Colloid Interface Sci., 407 (2013) 22–28.
[51] B.S. Inbaraj, T.-Y. Tsai, B.-H. Chen, Synthesis, characterization and antibacterial activity of superparamagnetic nanoparticles modified with glycol chitosan, Sci. Technol. Adv. Mater., 13 (2012) 015002.
[52] W. Jiang, H. Mashayekhi, B. Xing, Bacterial toxicity comparison between nano- and micro-scaled oxide particles, Environ. Pollut., 157 (2009) 1619–1625.
[53] M. Ul-Islam, A. Shehzad, S. Khan, W.A. Khattak, M.W. Ullah, J.K. Park, Antimicrobial and biocompatible properties of nanomaterials, J. Nanosci. Nanotechnol., 14 (2014) 780–791.
[54] S. Khan, M. Ul-Islam, W.A. Khattak, M.W. Ullah, J.K. Park, Bacterial cellulose-titanium dioxide nanocomposites: nanostructural characteristics, antibacterial mechanism, and biocompatibility, Cellulose, 22 (2015) 565–579.
[55] C. Umamaheswari, A. Lakshmanan, N.S. Nagarajan, Green synthesis, characterization and catalytic degradation studies of gold nanoparticles against congo red and methyl orange, J. Photochem. Photobiol. B., 178 (2018) 33–39.
[56] N. Gupta, H.P. Singh, R.K. Sharma, Metal nanoparticles with high catalytic activity in degradation of methyl orange: an electron relay effect, J. Mol. Catal. Chem., 335 (2011) 248–252.
[57] M. Hakamada, F. Hirashima, M. Mabuchi, Catalytic decoloration of methyl orange solution by nanoporous metals, Catal. Sci. Technol., 2 (2012) 1814–1817.
[58] K. Naseem, Z.H. Farooqi, R. Begum, A. Irfan, Removal of Congo red dye from aqueous medium by its catalytic reduction using sodium borohydride in the presence of various inorganic nano-catalysts: a review, J. Clean. Prod., 187 (2018) 296–307.
[59] T.R. Mandlimath, B. Gopal, Catalytic activity of first row transition metal oxides in the conversion of p-nitrophenol to p-aminophenol, J. Mol. Catal. Chem., 350 (2011) 9–15.
[60] O.A. Zelekew, D.-H. Kuo, Synthesis of a hierarchical structured NiO/NiS composite catalyst for reduction of 4-nitrophenol and organic dyes, RSC Adv., 7 (2017) 4353–4362.